



ELSEVIER

Available online at www.sciencedirect.com

SCIENCE @ DIRECT®

Optics Communications 249 (2005) 595–609

OPTICS
COMMUNICATIONS

www.elsevier.com/locate/optcom

Gradient-index crystalline lens model: A new method for determining the paraxial properties by the axial and field rays

María Angeles Rama, María Victoria Pérez, Carmen Bao,
María Teresa Flores-Arias *, Carlos Gómez-Reino

GRIN Optics Group, Applied Physics Department, Faculty of Physics and Optics and Optometry School, University of Santiago, Campus Sur, 15782 Santiago de Compostela, Spain

Received 24 November 2004; received in revised form 17 January 2005; accepted 22 January 2005

Abstract

Gradient-index (GRIN) models of the human lens have received wide attention in optometry and vision sciences for considering the effect of inhomogeneity of the refractive index on the optical properties of the lens. This paper uses the continuous asymmetric bi-elliptical model to determine analytically cardinal elements, magnifications and refractive power of the lens by the axial and field rays in order to study the paraxial light propagation through the human lens from its GRIN nature.

© 2005 Elsevier B.V. All rights reserved.

PACS: 42.66.-p; 42.66.Ct

1. Introduction

The most common models of the human crystalline lens are those found in the standard schematic eyes and they represent the optical structure by spherical and/or aspherical surfaces and constant refractive index. Schematic eye mod-

els are used to estimate basic optical properties of the eye such paraxial properties, ocular aberrations, etc. [1–5]. All of those models have the weakness that they do not use a variable refractive index and therefore do not accurately represent the optical structure of the lens.

To understand the effect of inhomogeneity of the refractive index within the lens on the optical properties of the lens and then on the eye as a whole, we need understand the role of the gradient-index (GRIN) structure in optical quality of the lens. It is clear that the GRIN structure may play a primary role in paraxial domain since it

* Corresponding author. Tel.: +34 981 563100; fax: +34 981 521984.

E-mail addresses: facgrc@usc.es (C. Gómez-Reino), famaite@usc.es (M.T. Flores-Arias).

URL: <http://www.usc.es/grinteam> (C. Gómez-Reino).

permits increase in the refractive power of the lens, which, otherwise, would be too low due to small differences in refractive index between adjacent biological media having a high water content. However, the GRIN structure may play a secondary role in aberrations since its contribution likely to be small [6–9].

In the optical modelling of the crystalline lens of the human eye, two different models are used. These are the shell and continuous GRIN models. In the shell or laminated model, the gradient index profile is represented by a finite and discrete set of concentric shells, with a constant refractive index in each shell [10–13]. In the construction of such a model, it is necessary to decide the number of shells, how the refractive index varies from shell to shell, and the value of curvature of the surface of each model. Once the shell structure is established, paraxial ray-tracing can be used to determine the lens power. For the continuous GRIN model the refractive index profile is represented by continuous iso-indicial surfaces [14–20]. Four types of continuous model depending on the external shape of the lens and the internal iso-indicial surfaces can be described. For the first two types the refractive index distribution is represented by elliptical iso-indicial surfaces that are concentric with the lens surfaces. The first type assumes symmetric iso-indicial surfaces. The second an asymmetric type in which the posterior curvature of any iso-indicial surface is greater than the anterior in such a way that, at the equatorial plane of joining, the iso-indicial surface is smooth and continuous. The first two types have also been proposed to describe the rabbit and the cat lenses [21,22]. The third type is a modified version of the second type, in which the iso-indicial surfaces remain asymmetric ellipsoids, but the surfaces of the lens are no longer iso-indicial contours [15]. The last type is more general, i.e., it is allowed any conicoid surface shape and a non-smooth joint at the equator [23,24]. The second and the third types provide a closest simulation to the real situation of the set of models provided. Ray tracing and ray path methods are used to calculate lens refractive power in continuous GRIN models. A more detailed information on lens models can be found in Ref. [25].

Recently, in the framework of the two asymmetric bi-elliptical types of the continuous GRIN

model, Pérez et al. [26] have found analytical expressions in the paraxial domain by approximating the gradient parameter that characterizes the refractive index distribution and the axial and field rays [27] that describe the light propagation (as well as the weak inhomogeneity condition) for a small variation in the gradient parameter over a defined wavelength distance. These rays were defined by Luneburg in order to facilitate the study of paraxial light propagation and aberration in GRIN media. Then, the aim of this paper, as a first step, is to find analytical expressions for locations of the cardinal elements, for the magnifications and for refractive power in order to know and to analyse the paraxial properties of the human lens from its GRIN nature in terms of the axial and field rays. The new method has the power to add new insights or predictions on a GRIN model of the lens in such a way that, dependences on thickness and on radius of the refractive power provide predictions on refractive index profile changes in the crystalline lens with age [28], and sign of derivative of the refractive power respect to thickness provides new insights on the lens paradox [29]. Explicit expressions for every one of the third-order aberrations in terms of the axial and field rays can be derived and analysed and no ray tracing methods are required [27–30].

2. Statement of the problem

For the asymmetric bi-elliptical model, the refractive index profile at any point in the sagittal section of the lens can be written as a power series [17]

$$n(y, z) = \sum_{j=0}^{\infty} c_j f^j(y, z), \quad (1)$$

where c_j are coefficients of the power series and

$$f(y, z) = \frac{(z - a_1)^2}{a_i^2} + \frac{y^2}{b^2} \quad (2)$$

with $i = 1$ for the front part ($0 \leq z \leq a_1$) of the lens, and $i = 2$ for the back part ($a_1 \leq z \leq d$) of the lens. The thickness of the lens along the z -axis is $d = a_1 + a_2$, b is the common semiaxis of ellipses along the y -axis and a_1 and a_2 are the semiaxes along

the z -axis of the asymmetric bi-elliptical iso-indicial curves (Fig. 1). $f(y, z)$ is defined so that, at the outer surface of the iso-indicial profile, it becomes unity.

If the central index is n_c and the edge index is n_e , from Eqs. (1) and (2), we have the following conditions:

$$n_c = c_0, \tag{3a}$$

$$n_e = \sum_{j=0}^{\infty} c_j \tag{3b}$$

and then

$$\Delta n = \sum_{j=1}^{\infty} c_j, \tag{4}$$

where Δn is the difference in refractive index between the edge and the centre of the lens.

To apply the well known results, in the paraxial domain, applied to GRIN optics, to a crystalline lens, we can now write Eq. (1) as [26]

$$n(y, z) = n_0(z) \left[1 - \frac{g^2(z)}{2} y^2 \right], \tag{5}$$

where $n_0(z)$ is the refractive index along the z -axis and $g(z)$ is the gradient parameter which character-

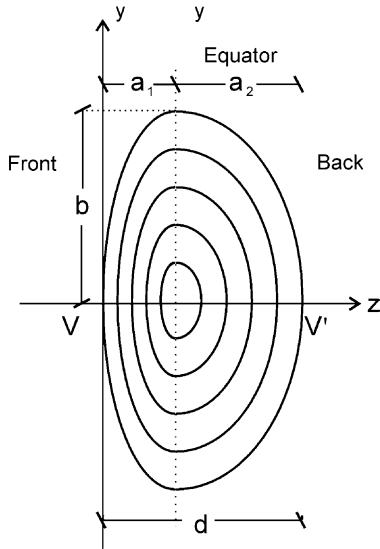


Fig. 1. The refractive index distribution of the crystalline lens in the sagittal section, represented as bi-elliptical iso-indicial curves joined at the equator. For the iso-indicial curves the origin of the axes is at V .

izes the refractive index distribution. As we are only concerned with GRIN nature of the lens, in paraxial domain, all terms higher than the second order in y , for the refractive index, are aberration terms and are rejected.

For the front part of the lens, we have

$$g_f^2(z) = - \frac{\sum_{j=1}^{\infty} 2j c_j \left[\frac{z-a_1}{a_1} \right]^{2(j-1)}}{b^2 n_{0f}(z)}, \tag{6}$$

where

$$n_{0f}(z) = n_f(y, z)|_{y=0} = \sum_{j=0}^{\infty} c_j \left(\frac{z-a_1}{a_1} \right)^{2j} \tag{7}$$

and for the back part of the lens

$$g_b^2(z) = - \frac{\sum_{j=1}^{\infty} 2j c_j \left[\frac{z-a_1}{a_2} \right]^{2(j-1)}}{b^2 n_{0b}(z)}, \tag{8}$$

where

$$n_{0b}(z) = n_b(y, z)|_{y=0} = \sum_{j=0}^{\infty} c_j \left(\frac{z-a_1}{a_2} \right)^{2j}. \tag{9}$$

Subindices f and b denote front and back parts of the lens, respectively.

In particular, the values of the gradient parameter at the centre and the edges of the z -axis are given by

$$g_c^2 = g_f^2(a_1) = g_b^2(a_1) = - \frac{2c_1}{n_c b^2}, \tag{10a}$$

$$g_c^2 = g_f^2(0) = g_b^2(d) = - \frac{2 \sum_{j=1}^{\infty} j c_j}{b^2 n_e}, \tag{10b}$$

where Eqs. (3) have been used.

On the other hand, it is well known that the light propagation in a GRIN medium can be studied by using the axial and field rays, two linearly independent solutions of the paraxial ray equation, in such a way that any paraxial ray can be expressed as a linear combination of these two rays defined by Luneburg [27]. For small variation in $g(z)$ over a wavelength distance, the weak inhomogeneity condition says [26]

$$\frac{|\dot{g}(z)|}{g^2(z)} \ll 1, \tag{11}$$

where a dot denotes a derivative with respect to z and the positions H_a and H_f and the slopes \dot{H}_a and \dot{H}_f of the axial and field rays in the crystalline lens can be expressed as

$$H_{af}(z) = \left[\frac{g_f(z)}{g_c} \right]^{1/2} \left[1 - \frac{g_f^2(z)z^2}{6} \right] z, \quad (12a)$$

$$H_{ff}(z) = \left[\frac{g_c}{g_f(z)} \right]^{1/2} \left\{ 1 - \frac{g_f^2(z)}{2} z^2 + \frac{\dot{g}_c g_f(z)}{2g_c^2} \left[1 - \frac{g_f^2(z)z^2}{6} \right] z \right\}, \quad (12b)$$

$$\dot{H}_{af}(z) = \left[\frac{g_f(z)}{g_c} \right]^{1/2} \left\{ 1 - \frac{g_f^2(z)}{2} z^2 - \frac{\dot{g}_f(z)}{2g_f(z)} \left[1 - \frac{g_f^2(z)z^2}{6} \right] z \right\}, \quad (12c)$$

$$\begin{aligned} \dot{H}_{ff}(z) = [g_c g_f(z)]^{1/2} & \left\{ \frac{1}{2} \left[\frac{\dot{g}_c}{g_c^2} - \frac{\dot{g}_f(z)}{g_f^2(z)} \right] \left[1 - \frac{g_f^2(z)z^2}{2} \right] \right. \\ & \left. - \left[1 + \frac{\dot{g}_c \dot{g}_f(z)}{4g_c^2 g_f^2(z)} \right] \left[1 - \frac{g_f^2(z)z^2}{6} \right] g_f(z) z \right\} \end{aligned} \quad (12d)$$

for the front part and

$$H_{ab}(z) = \left[\frac{g_b(z)}{g_c} \right]^{1/2} \left[1 - \frac{g_b^2(z)z^2}{6} \right] z, \quad (12e)$$

$$H_{fb}(z) = \left[\frac{g_c}{g_b(z)} \right]^{1/2} \left\{ 1 - \frac{g_b^2(z)}{2} z^2 + \frac{\dot{g}_c g_b(z)}{2g_c^2} \left[1 - \frac{g_b^2(z)z^2}{6} \right] z \right\}, \quad (12f)$$

$$\dot{H}_{ab}(z) = \left[\frac{g_b(z)}{g_c} \right]^{1/2} \left\{ 1 - \frac{g_b^2(z)}{2} z^2 - \frac{\dot{g}_b(z)}{2g_b(z)} \left[1 - \frac{g_b^2(z)z^2}{6} \right] z \right\}, \quad (12g)$$

$$\begin{aligned} \dot{H}_{fb}(z) = [g_c g_b(z)]^{1/2} & \left\{ \frac{1}{2} \left[\frac{\dot{g}_c}{g_c^2} - \frac{\dot{g}_b(z)}{g_b^2(z)} \right] \left[1 - \frac{g_b^2(z)z^2}{2} \right] \right. \\ & \left. - \left[1 + \frac{\dot{g}_c \dot{g}_b(z)}{4g_c^2 g_b^2(z)} \right] \left[1 - \frac{g_b^2(z)z^2}{6} \right] g_b(z) z \right\} \end{aligned} \quad (12h)$$

for the back part, with boundary conditions

$$H_{af}(0) = 0, \quad H_{af}(a_1) = H_{ab}(a_1), \quad (13a)$$

$$H_{ff}(0) = 1, \quad H_{ff}(a_1) = H_{fb}(a_1), \quad (13b)$$

$$\dot{H}_{af}(0) = 1, \quad \dot{H}_{af}(a_1) = \dot{H}_{ab}(a_1), \quad (13c)$$

$$\dot{H}_{ff}(0) = 0, \quad \dot{H}_{ff}(a_1) = \dot{H}_{fb}(a_1), \quad (13d)$$

and with Lagrange's invariant

$$H_{f(b)}(z) \dot{H}_{a(b)}(z) - \dot{H}_{f(b)}(z) H_{a(b)}(z) = 1 \quad (14)$$

for the specific boundary conditions given by Eqs. (13).

Likewise, matrices have been used for studying paraxial light propagation in GRIN lenses if the axial and field rays are known [31]. Then, using matrix methods it is possible to analyse paraxial light propagation in the crystalline lens as follows [12]:

$$\begin{pmatrix} y(z) \\ \dot{y}(z) \end{pmatrix} = \begin{pmatrix} H_{f(b)}(z) & H_{a(b)}(z) \\ \dot{H}_{f(b)}(z) & \dot{H}_{a(b)}(z) \end{pmatrix} \begin{pmatrix} y_0 \\ \dot{y}_0 \end{pmatrix} = H(z) \begin{pmatrix} y_0 \\ \dot{y}_0 \end{pmatrix} \quad (15)$$

such that $\det H(z) = 1$.

In Eq. (15), y_0 and \dot{y}_0 are, respectively, the position and slope of a paraxial ray at the input of the front part of the lens and $\dot{H}_{f(b)}$ and $\dot{H}_{a(b)}$ are given by Eqs. (12). Solutions of this matrix equation express the position $y(z)$ and the slope $\dot{y}(z)$ of the paraxial ray at any point of the lens as a linear combination of the position and the slope of the axial and field rays.

3. Cardinal elements: GRIN refractive power

The cardinal elements locations of the crystalline lens are dependent on the curvature radii of the front and back surfaces, the refractive index differences at the aqueous-lens and vitreous-lens interfaces and the refractive index within the lens. These locations may have a significant effect on the lens refractive power. As commented previously, here we are only concerned with the dependence of the lens which arises from its GRIN nature and the eye lens can be replaced by a GRIN lens of thickness d and radius b (Fig. 2).

The back refractive power of the lens is expressed as [32]

$$P'_G = \frac{n'_1}{f'} \quad (16a)$$

and the back vertex power is written as

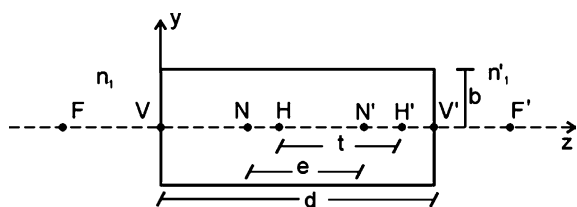


Fig. 2. The crystalline lens as a GRIN lens with parallel faces and thickness d .

$$P'_{V'} = \frac{n'_1}{f'}, \quad (16b)$$

where n'_1 is the refractive index of the medium in the image side of the GRIN lens and f' and l' are the back focal and back vertex focal distances, given by

$$f' = H'F' = -\frac{n'_1}{n_e \dot{H}_{fb}(d)}, \quad (17a)$$

$$l' = V'F' = -\frac{n'_1 H_{fb}(d)}{n_e \dot{H}_{fb}(d)} = f' H_{fb}(d). \quad (17b)$$

From Eqs. (17), it follows that back focal and back vertex focal distances depend on the position and slope of the field ray evaluated at d . In particular, axial and field rays at the edge of the crystalline lens can be written as

$$H_{ab}(d) = d \cdot \left(1 - \frac{g_c^2 \cdot d^2}{6}\right), \quad (18a)$$

$$\begin{aligned} H_{fb}(d) &= 1 - \frac{g_c^2 d^2}{2} + \frac{\dot{g}_c d}{2g_c} \left(1 - \frac{g_c^2 d^2}{6}\right) \\ &= 1 - \frac{g_c^2 d^2}{2} + \frac{\dot{g}_c}{2g_c} \cdot H_{ab}(d), \end{aligned} \quad (18b)$$

$$\begin{aligned} \dot{H}_{ab}(d) &= 1 - \frac{g_c^2 d^2}{2} - \frac{\dot{g}_c d}{2g_c} \left(1 - \frac{g_c^2 d^2}{6}\right) \\ &= 1 - \frac{g_c^2 d^2}{2} - \frac{\dot{g}_c}{2g_c} \cdot H_{ab}(d), \end{aligned} \quad (18c)$$

$$\begin{aligned} \dot{H}_{fb}(d) &= -g_c d \left(1 - \frac{g_c^2 d^2}{6}\right) \left(g_c + \frac{\dot{g}_c}{4g_c^3}\right) \\ &= -\left(g_c^2 + \left(\frac{\dot{g}_c}{2g_c}\right)^2\right) \cdot H_{ab}(d), \end{aligned} \quad (18d)$$

where Eqs. (12e)–(12h) have been used.

In above equations, the relationship between the slope of the gradient parameter and this parameter at the edge is given by [26]

$$\frac{\dot{g}_c}{2g_c} = -\frac{n_e \cdot \sum_{j=2}^{\infty} j(j-1)c_j - \left[\sum_{j=1}^{\infty} j c_j\right]^2}{2dn_e \cdot \sum_{j=1}^{\infty} j c_j}. \quad (19)$$

Eq. (19) says that the slope of the gradient parameter at the edge is inversely proportional to the thickness of the lens.

Likewise, Eqs. (17) provide the position of the back focus from the rear principal point and the vertex V' , respectively. Substitution of Eqs. (17) into Eqs. (16) provides

$$P'_G = -n_e \cdot \dot{H}_{fb}(d), \quad (20a)$$

$$P'_{V'} = -n_e \frac{\dot{H}_{fb}(d)}{H_{fb}(d)} = \frac{P'_G}{H_{fb}(d)}. \quad (20b)$$

From Eqs. (20) it follows that the back refractive power and back vertex power depend on the edge index and the values of the position and slope of the field ray at d . If the refractive index is constant along the axis and $c_j = 0$ for $j > 1$, the lens power reduces to the power of the Wood lens when the fourth term in g_c is neglected [33].

On the other hand, the positions of the remainder back cardinal points can be found as follows: the position of the back principal point H' with respect to V' is expressed as [32]

$$V'H' = l' - f' = \frac{n'_1 [H_{fb}(d) - 1]}{P'_G}, \quad (21)$$

where Eqs. (17) have been used.

The position of the back nodal point N' can be written as

$$V'N' = \frac{n_1 - n'_1 H_{fb}(d)}{n_e \dot{H}_{fb}(d)} = \frac{n'_1 H_{fb}(d) - n_1}{P'_G}, \quad (22)$$

where n_1 is the refractive index of the medium on the object side of the GRIN lens and Eq. (20a) has been used.

From Eqs. (21) and (22) it follows that the separation between back principal and nodal points is given by

$$H'N' = -\frac{n_1 - n'_1}{P'_G}. \quad (23)$$

Therefore, Eq. (22) reduces to Eq. (21) and nodal and principal points coincide as $n_1 = n'_1$.

In the same way, the positions of the front cardinal points are written for the crystalline lens as [32]

$$f = HF = \frac{n_1}{n_e \dot{H}_{fb}(d)}, \quad (24a)$$

$$l = VF = \frac{n_1 \dot{H}_{ab}(d)}{n_e \dot{H}_{fb}(d)} = f \dot{H}_{ab}(d), \quad (24b)$$

$$VN = -\frac{n'_1 - n_1 \dot{H}_{ab}(d)}{n_e \dot{H}_{fb}(d)}. \quad (24c)$$

Eqs. (24a) and (24b) denote the front focal and front vertex focal distances, respectively, and they give the position of the front focus from the front principal point and the vertex V of the lens. Eq. (24c) gives the position of the front nodal point from the vertex V .

The front refractive power and front vertex power are expressed, respectively, as

$$P_G = -\frac{n_1}{f} = -n_e \dot{H}_{fb}(d) = P'_G, \quad (25a)$$

$$P_V = -\frac{n_1}{l} = -n_e \frac{\dot{H}_{fb}(d)}{\dot{H}_{ab}(d)} = \frac{P'_G}{\dot{H}_{ab}(d)} = \frac{H_{fb}(d)}{\dot{H}_{ab}(d)} P'_{V'}, \quad (25b)$$

where Eqs. (20a) and (24a), (24b) have been used.

From Eqs. (25) it follows that both powers depend on the edge index and the values at d of the slopes of the axial and field rays. Front refractive power coincides with the corresponding back magnitude and the coincidence between front and back vertex powers occurs as the value of the slope of gradient parameter at the vertex is neglected, that is, as $\dot{H}_{ab}(d) = H_{fb}(d)$.

Furthermore, the position of the front principal point is given by

$$VH = l - f = -\frac{n_1 [\dot{H}_{ab}(d) - 1]}{P'_G} \quad (26)$$

and the distance between front principal and nodal points is written as

$$HN = \frac{n_1 - n'_1}{P'_G} \quad (27)$$

where Eqs. (24c) and (26) have been used.

From Eqs. (26) and (27) it follows that front nodal and principal points coincide and that front and back principal points are located at the same distances from the vertices V and V' , respectively, as $n_1 = n'_1$ and $\dot{H}_{ab}(d) = H_{fb}(d)$.

Finally, separation between principal points can be written as (see Fig. 2)

$$t = HH' = d - VH + V'H'. \quad (28)$$

Inserting Eqs. (21) and (26) into Eq. (28) we obtain

$$t = d - \frac{n_1 + n'_1 - n_1 \dot{H}_{ab}(d) - n'_1 H_{fb}(d)}{P'_G} \quad (29)$$

when $n_1 = n'_1$, Eq. (29) becomes

$$t = d - n_1 \frac{[2 - \dot{H}_{ab}(d) - H_{fb}(d)]}{P'_G} \quad (30)$$

and if $\dot{H}_{ab}(d) = H_{fb}(d)$, Eq. (30) reduces to

$$t = d - 2n_1 \frac{[1 - H_{fb}(d)]}{P'_G}. \quad (31)$$

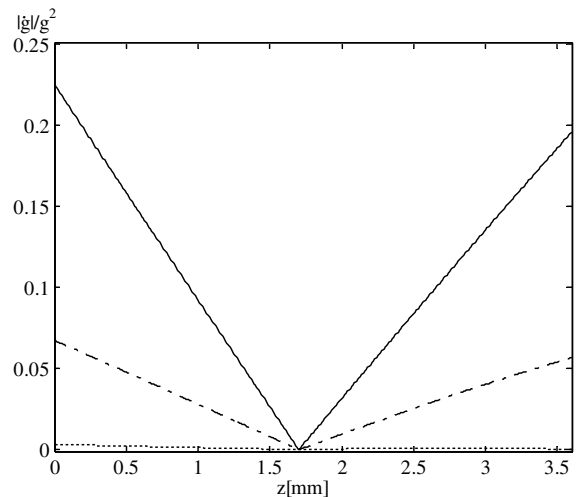


Fig. 3. The weak inhomogeneity condition. Calculations have been made for $b=4.5$ mm, $d=3.6$ mm ($a_1=1.7$ mm, $a_2=1.9$ mm), $c_0=1.406$ and $c_1=-0.02$ (solid curve); $c_1=-0.0201$ and $c_2=0.0001$ (dashed curve) and $c_1=-0.0201416$, $c_2=0.0001423$ and $c_3=-0.0000007$ (dotted curve).

Similarly, separation between nodal points is given by

$$e = NN' = d - VN + V'N'$$

$$= d - \frac{n_1 + n'_1 - n_1 \dot{H}_{ab}(d) - n'_1 \dot{H}_{fb}(d)}{P'_G}, \quad (32)$$

where Eqs. (22) and (24c) have been used.

We obtain a well known result in geometrical optics that it says the distance between the nodal points is equal to the distance between the principal points and when $n_1 = n'_1$ the nodal and the principal points coincide.

4. Magnifications

In treatments on magnifications of the crystalline lens, there is no consideration of its GRIN nature and, hence, there is no possibility for knowing the angular and position transformations of the rays induced by the refractive index profile.

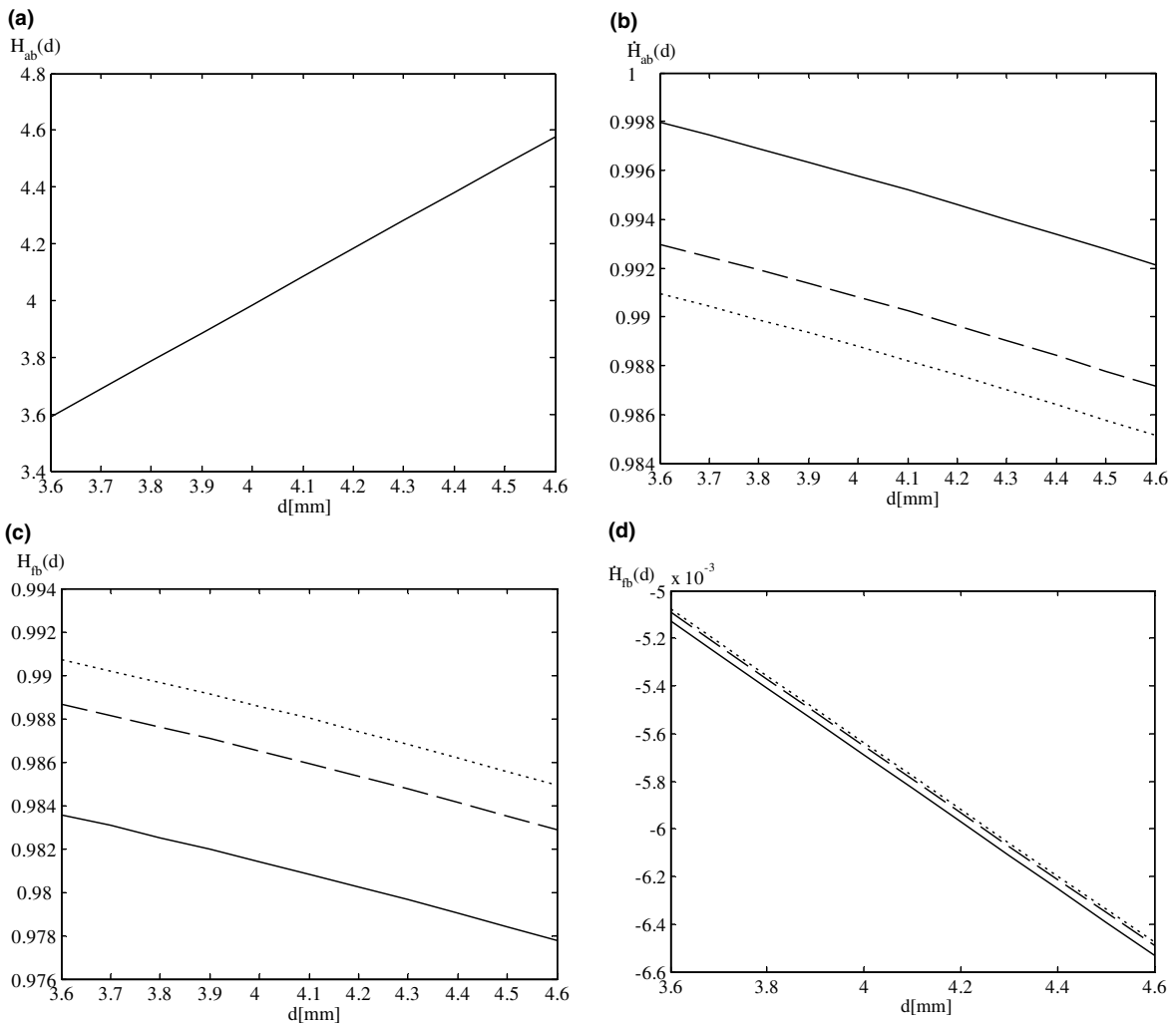


Fig. 4. Position and slope of the axial ray (a) and (b) and of the field ray (c) and (d), respectively, with lens thickness. Calculations have been made for b and c_j values of Fig. 3. Note that in (a) all lines for different coefficients are superimposed.

Transversal, longitudinal and angular magnifications are significant magnitudes in an optical system since they give such position and angle transformations of rays propagating through it. In particular, transversal and angular magnifications for the crystalline lens from its GRIN nature take the forms [32]

$$m_t = \frac{n_1}{n_1 \dot{H}_{ab}(d) + n_e d_1 \dot{H}_{fb}(d)} = \frac{n'_1 H_{fb}(d) + n_e d'_1 \dot{H}_{fb}(d)}{n'_1}, \quad (33a)$$

$$m_a = \frac{n_1 \dot{H}_{ab}(d) + n_e d_1 \dot{H}_{fb}(d)}{n'_1} = \frac{n_1}{n'_1 H_{fb}(d) + n_e d'_1 \dot{H}_{fb}(d)}, \quad (33b)$$

where d_1 and d'_1 are object and image distances measured from vertices V and V' , respectively.

Inserting Eqs. (20) and (25) into Eqs. (33) we have

$$m_t = \frac{n_1 P_V}{(n_1 - d_1 P_V) P'_G} = \frac{(n'_1 - d'_1 P'_V) P'_G}{n'_1 P'_V}, \quad (34a)$$

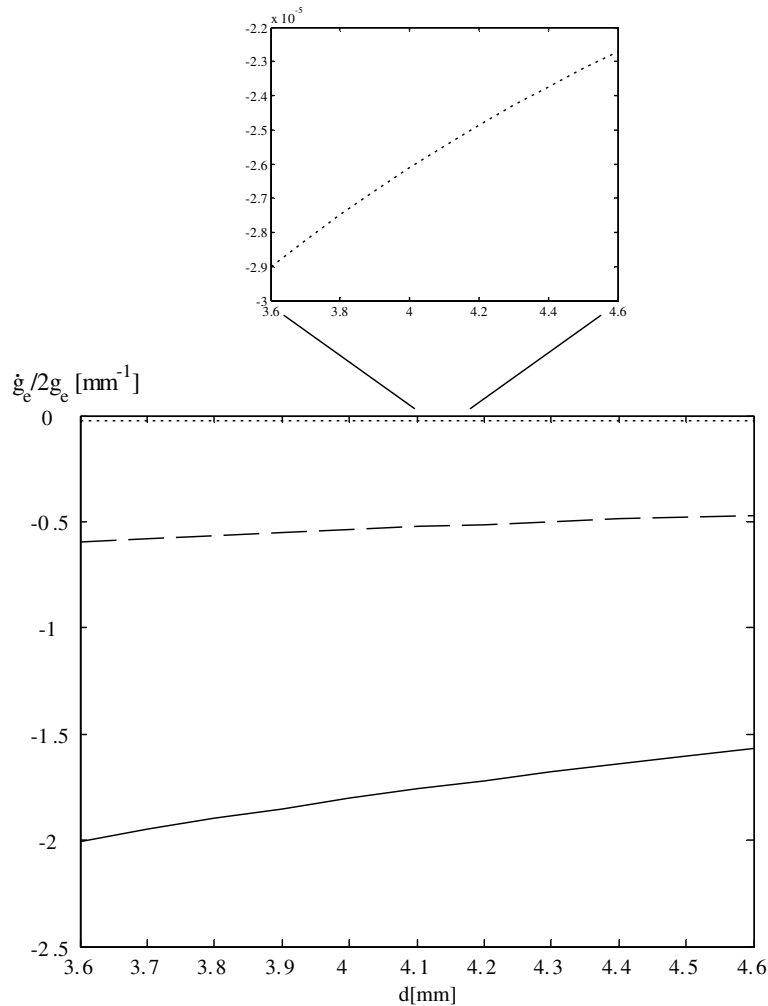


Fig. 5. Slope of the gradient parameter versus thickness. Calculations have been made for b and c_j values of Fig. 3. Behaviour for four coefficients is enlarged.

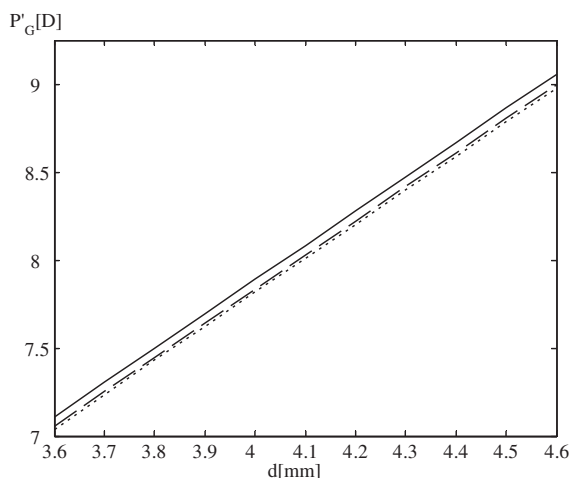


Fig. 6. Back refractive power versus thickness. Calculations have been made for b and c_j values of Fig. 3.

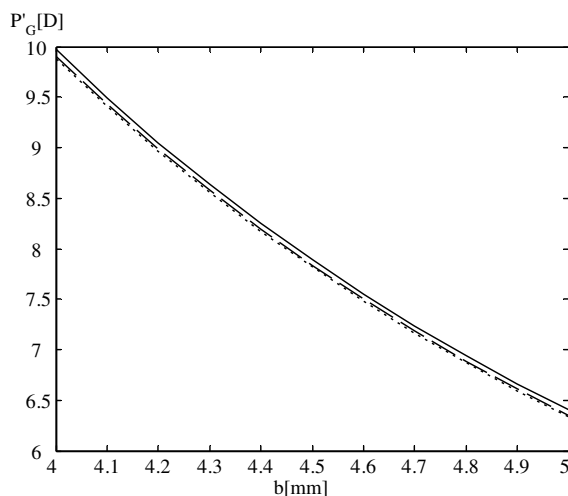


Fig. 8. Back refractive power versus equatorial radius. Calculations have been made for c_j values of Fig. 3 and $d = 4$ mm.

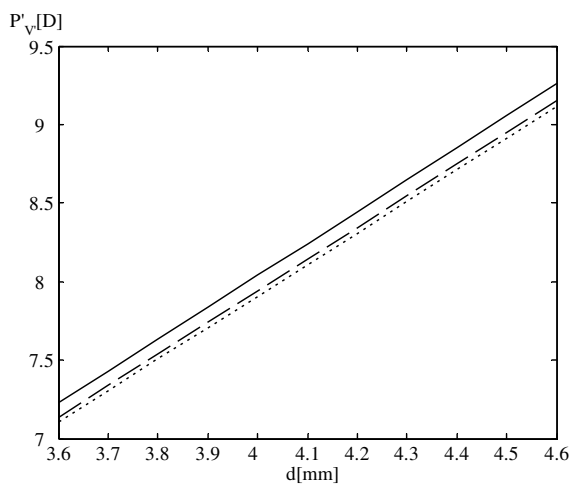


Fig. 7. Back vertex power versus thickness. Calculations have been made for b and c_j values of Fig. 3.

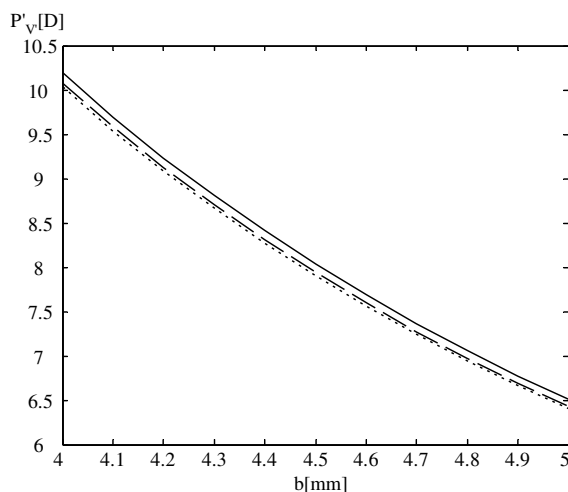


Fig. 9. Back vertex power versus equatorial radius. Calculations have been made for c_j values of Fig. 3 and $d = 4$ mm.

$$m_a = \frac{(n_1 - d_1 P_V) P'_G}{n'_1 P_V} = \frac{n_1 P'_V}{(n'_1 - d'_1 P'_V) P'_G} \quad (34b)$$

note that $m_t = m_a^{-1}$ as $n_1 = n'_1$.

In the same way, expression for the longitudinal magnification is given by [32]

$$m_l = - \frac{n_1 n'_1}{[n_e d_1 \dot{H}_{fb}(d) + n_1 \dot{H}_{ab}(d)]^2} = - \frac{[n'_1 H_{fb}(d) + n_e d'_1 \dot{H}_{fb}(d)]^2}{n_1 n'_1} \quad (35)$$

last equation can be written in terms of refractive powers as

$$m_l = - \frac{n_1 n'_1 P_V^2}{(n_1 - d_1 P_V)^2 P_G^2} = - \frac{(n'_1 - d'_1 P'_V)^2 P_G^2}{n_1 n'_1 P_V^2} \quad (36)$$

From Eqs. (34) and (35), it follows that the relationship between magnifications is expressed as

$$m_t = -m_a m_l. \tag{37}$$

Eq. (37) for $n_1 = n'_1$ reduces to

$$m_t^2 = -m_l \text{ or } m_a^2 m_l = -1. \tag{38}$$

Eqs. (37) and (38) are other well known results in geometrical optics.

5. Results

In order to analyse the paraxial behaviour of the crystalline lens from its GRIN nature, we have

considered a lens characterized by a transverse parabolic refractive index distribution in the sagittal section, given by Eq. (5), modulated by a longitudinal refractive index along the optical axis containing up to a 6th order in z . Values of central refractive index of 1.406 and edge index of 1.386 were taken from the Gullstrand schematic eye. The coefficients c_j of the power series in the refractive index profile can be found by Eqs. (3) taking into account the weak inhomogeneity condition. Fig. 3 shows this condition for two, three and four coefficients of the power series in the refractive

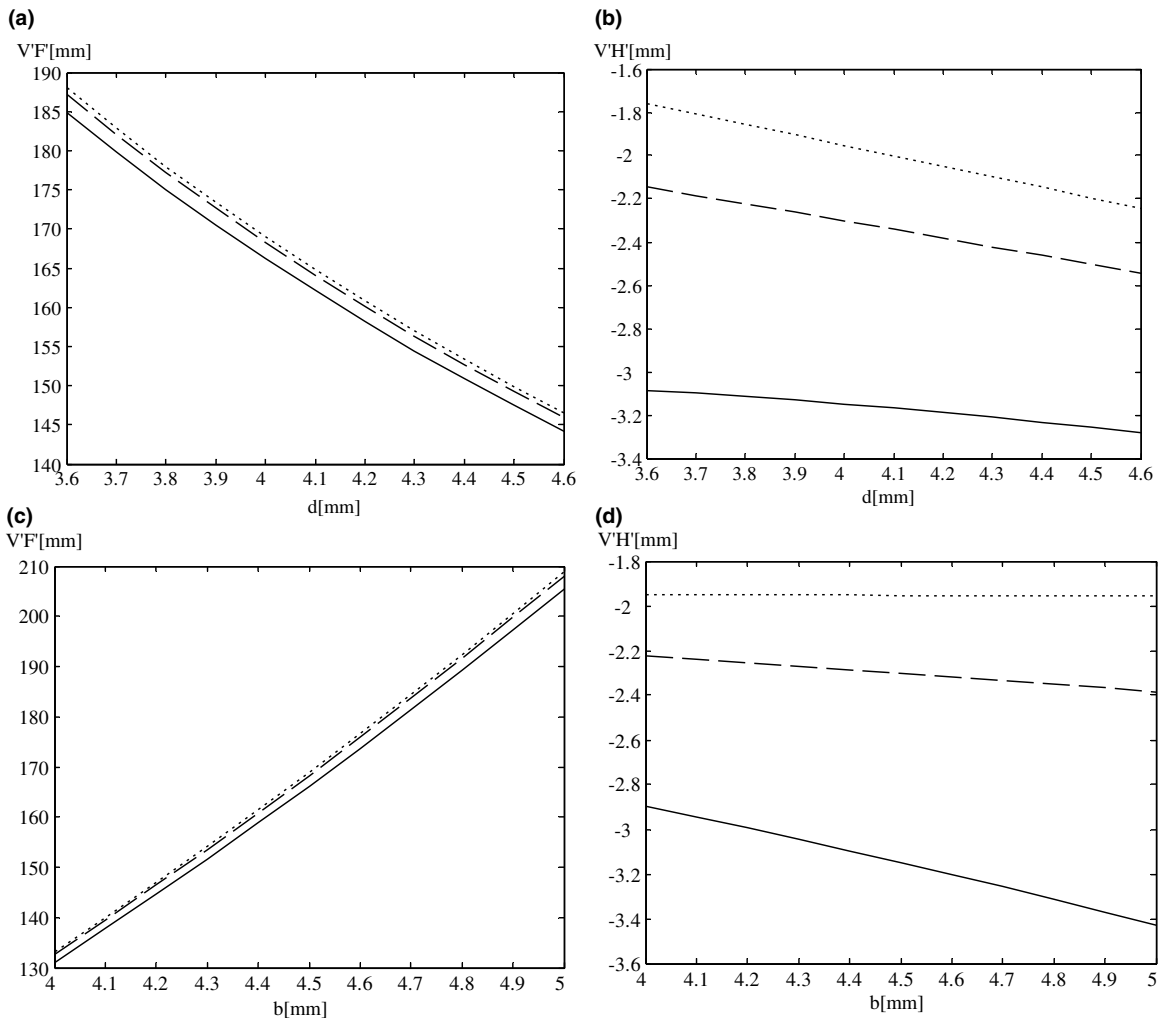


Fig. 10. Positions of the back focal (a) and principal (b) points, measured from back vertex, versus thickness and positions of the back focal (c) and principal (d) points versus equatorial radius. Calculations have been made for c_j values of Fig. 3.

index profile along the optical axis. The more coefficients we take into account, the better condition (11) is satisfied. As the paraxial properties of the lens depend on the values of the axial and field rays at the output face, we depict in Fig. 4 the variation of position and slope of these rays with thickness for two, three and four coefficients in the refractive index. Position of the axial rays increases with thickness and there is no dependence on the number of coefficients for the position of the axial ray increasing with thickness (Fig. 4(a)). However, the decrease of the slope of this ray

depends on the number of coefficients (Fig. 4(b)). Likewise, the slope of the ray for four coefficients is smaller than for three and two coefficients, respectively. In all cases, the angle between the ray and the optical axis at the output is close to $\pi/4$. Figs. 4(c) and (d) represent the variation of the position and slope of the field ray at the output with thickness. It can be seen that the position of the field ray decreases with the number of coefficients and this position is smaller for two coefficients than for three and four coefficients, respectively. On the other hand, the slope of the

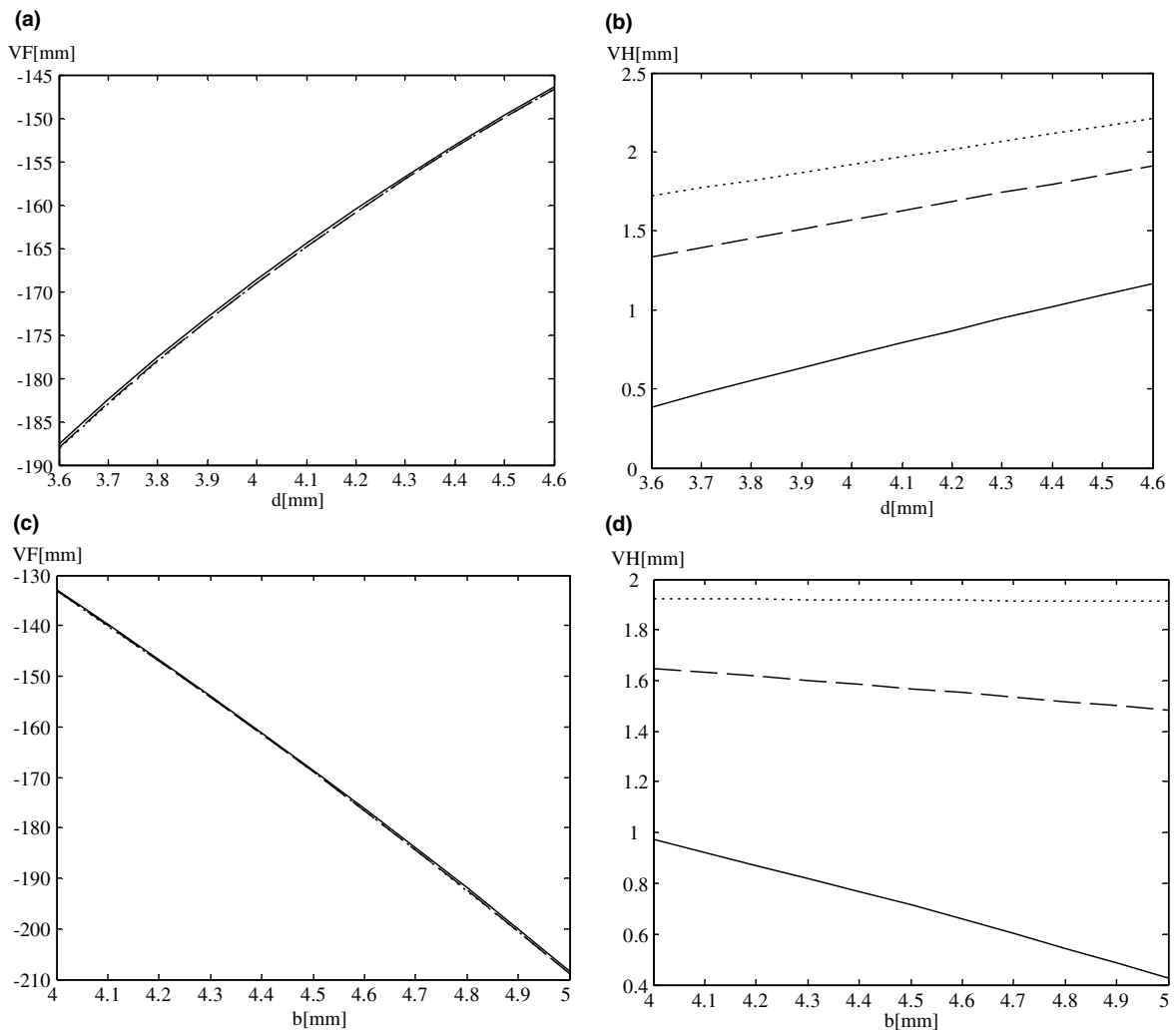


Fig. 11. Positions of the front focal (a) and principal (b) points, measured from front vertex, versus thickness and positions of the front focal (c) and principal (d) points versus equatorial radius. Calculations have been made for c_j values of Fig. 3.

field ray has almost the same behaviour for the highest orders of the index along axis (three and four coefficients) and it is higher than for the lowest order (two coefficients) of the refractive index. Direction of the field ray at the output is close to the optical axis. Fig. 5 shows the change in the slope of the gradient parameter referred to the gradient parameter at the edge with thickness for the above number of coefficients in the refractive index. In all cases, a slight increase occurs. Also, the value of the relationship between the slope of the gradient parameter and this parameter increases with the number of coefficients and it tends to zero for the highest number of coefficients. $\dot{g}_e/2g_e$ versus d is enlarged for four coefficients in order to reveal this behaviour. A linear increase of the crystalline lens back refractive power with thickness is shown in Fig. 6 for the different number of coefficients in the refractive index. The back refractive power is higher for two coefficients than for three and four coefficients in the refractive index. At the last two cases, the back refractive power achieves almost the same value. We depict in Fig. 7 variation of the back vertex power of the crystalline lens with thickness. A similar behaviour (as in Fig. 6) is shown altering both powers, it is measured from focus and vertex, respectively, by a value of approximately of 2 D between the thick-

ness of 3.6 and 4.6 mm. On the other hand, slightly higher values of the back vertex power are obtained in comparison to the values of the back refractive power for the different numbers of coefficients. Figs. 8 and 9 represent the back powers versus the equatorial radius of the lens for a lens thickness of 4 mm and for different number of coefficients in the refractive index. In both figures a decrease of about 3.5 D in the back power with b can be observed instead of an increase as in Figs. 6 and 7. The back refractive power and the back vertex power are higher for two coefficients than for three and four coefficients having almost the same behaviour for the highest orders of the refractive index along the optical axis. Figs. 10 and 11 represent the cardinal points positions of the crystalline lens, measured from vertices, versus d and b for $n_1 = n'_1$ (nodal and principal points coincide) and different number of coefficients in the refractive index along the axis. Figs. 10(a) and (b) depict positions of the back focal and principal points versus thickness, and Figs. 10(c) and (d) show these positions versus equatorial radius. Back focus moves away from back vertex as equatorial radius increases (Fig. 10(c)) and it has a reverse behaviour with thickness (Fig. 10(a)). In both cases, distances from the vertex to the focus are higher for three and four coefficients than for

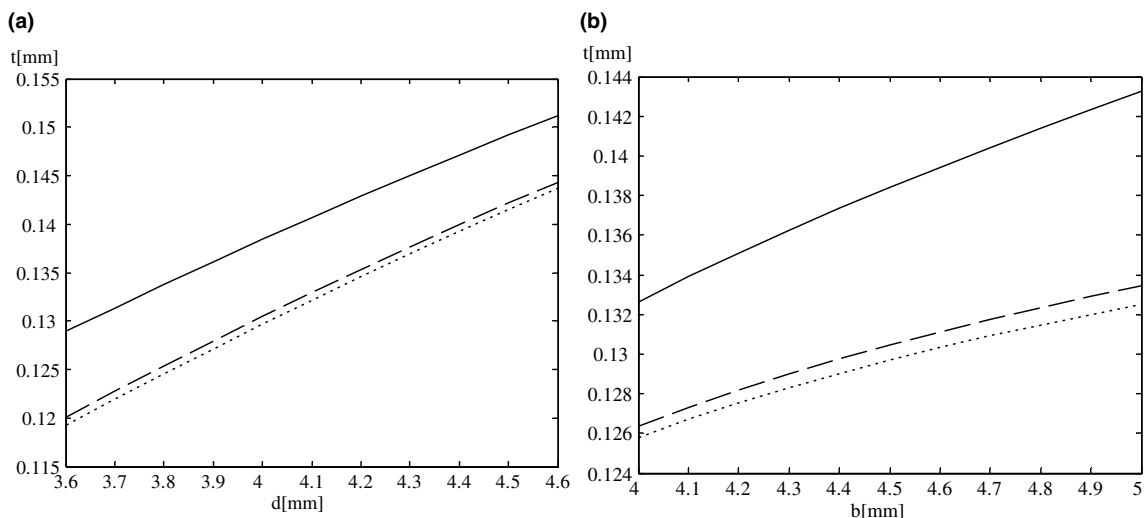


Fig. 12. Separation between principal points with thickness (a) and with equatorial radius (b). Calculations have been made for c_j values of Fig. 3.

two coefficients. Back principal point is located on the left of the back vertex and inside the lens as shown in Figs. 10(b) and (d). It moves away from the vertex as thickness and equatorial radius increase for all cases. Figs. 11(a) and (b) depict variation of the positions of the front focal and principal points with thickness and Figs. 11(c) and (d) show the variation of these positions with equatorial radius. Front focus moves away from front vertex as equatorial radius increases (Fig. 11(c)) and it moves back to front vertex as thickness increases (Fig. 11(a)). In both cases, a very weak dependence on the number of coefficients is

shown. Front principal point is located on the right of the front vertex and inside the crystalline lens for the three cases as seen in Figs. 11(b) and (d). Front principal point moves away from the vertex as thickness increases (Fig. 11(b)). However, front principal point moves back to the vertex as equatorial radius increases (Fig. 11(d)).

The variation of the separation between principal points with thickness and equatorial radius is represented in Fig. 12. Separation is higher for two coefficients than for three and four ones. Separation increases slightly with thickness and equatorial radius for the three cases. Figs. 13

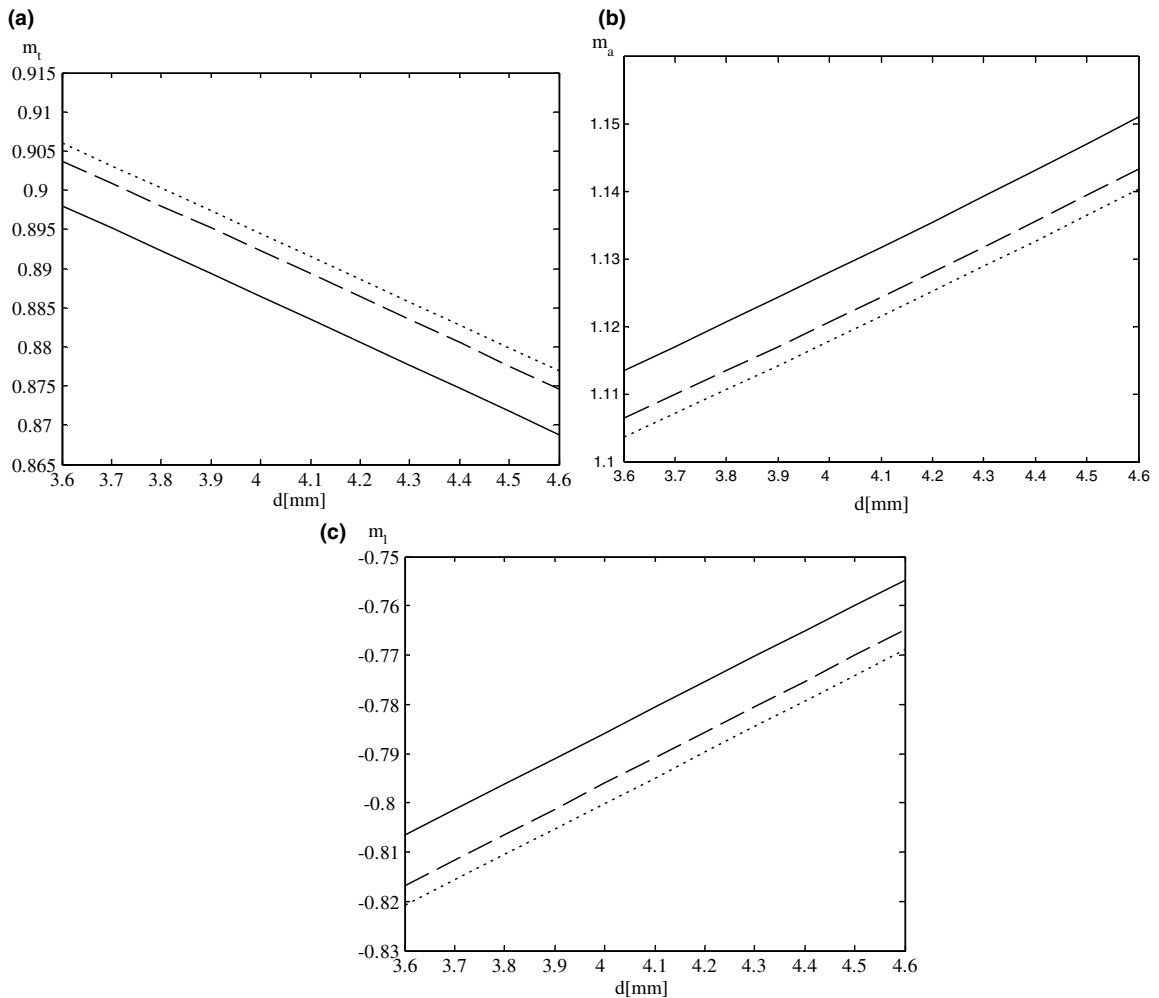


Fig. 13. Transversal (a), angular (b) and longitudinal (c) magnifications versus thickness. Calculations have been made for b and c_j values of Fig. 3.

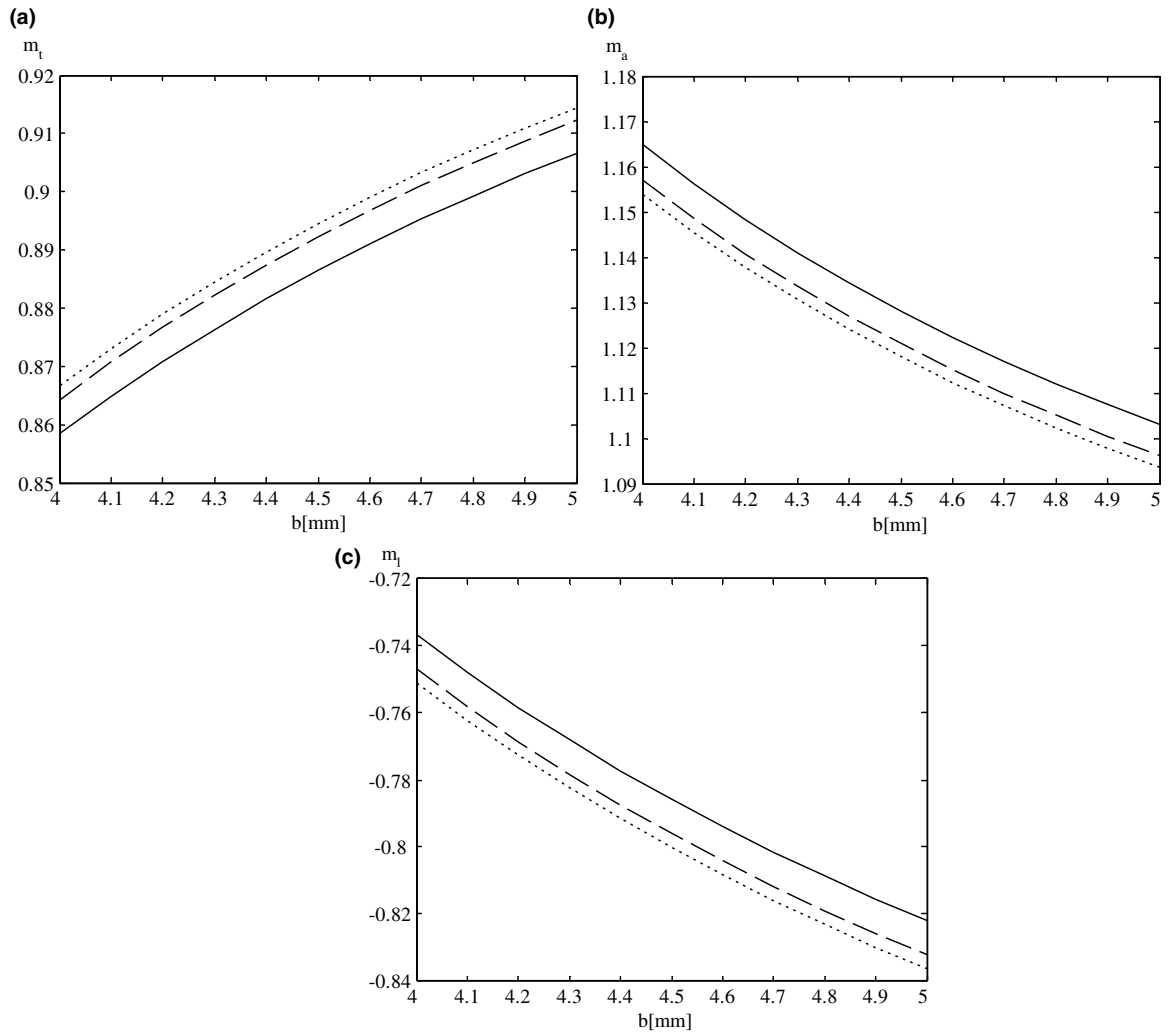


Fig. 14. Transversal (a), angular (b) and longitudinal (c) magnifications versus equatorial radius. Calculations have been made for c_j values of Fig. 3 and $d = 4$ mm.

and 14 depict magnifications versus d and b , for different number of coefficients and for a image distance $d'_1 = 16.08$ mm [34]. In all cases, a dependence of magnification on the number of coefficients is shown as d and b increase. Angular magnification is higher for two coefficients than for three and four coefficients in the refractive index as d and b increase. A reverse behaviour occurs for transverse and longitudinal magnifications. Angular magnification increases with d (Fig. 13(b)) and transverse and longitudinal magnifications decreases with d (Fig. 13(a) and

(c)). We have a reverse behaviour with b (Fig. 14).

6. Conclusions

Using the asymmetric elliptical model, we have presented analytical expressions for evaluating the paraxial properties of the human lens from its GRIN nature by the axial and field rays. In particular, cardinal elements location, magnifications and refractive power of a lens, with transverse parabolic

refractive index distribution in sagittal section modulated by a longitudinal refractive index along the z optical axis containing up to a 6th order in z , have been calculated as a function of the axial and field rays that describe paraxial light propagation through GRIN media. The values of c_j coefficients of the power series in the refractive index profile were evaluated from the central and edge indices as utilized in the Gullstrand schematic eye and from the weak inhomogeneity condition. Results show that the paraxial properties of the lens are sensitive to the form of the axial refractive index profile, specially for two coefficients, but the sensitivity decreases as the number of coefficients increases. On the other hand, an increase of 2 D and a decrease of 3.5 D of the power occurs as the thickness and the equatorial semidiameter vary between 3.6 and 4.6 mm and between 4 and 5 mm, respectively. Magnifications have been evaluated and it resulted in a well known relationship in geometrical optics as applied to the relationship between them. A very weak dependence of magnifications on the number of coefficients as thickness and equatorial radius of the crystalline increase has been shown. In short, paraxial properties of the eye lens from its GRIN nature have been easily evaluated by a new method in terms of the axial and field rays. The potential applications of such a method abound and the next steps will be the inclusion in our model of the curved end surfaces for the GRIN lens and the corneal component of the eye to determine the cardinal elements and the power of the whole eye and to evaluate the MTF as well as to compare our model with other ones available in the literature.

Acknowledgements

This work and the research of M.T. Flores-Arias were supported by the Ministerio de Educación y Ciencia, Spain, under contract FEDER/TIC 2003-03041. The GRIN Optics Group at USC is a NEMO/EU partner (Network of Excellence on Micro-Optics).

References

- [1] W. Lotmar, *J. Opt. Soc. Am.* 61 (1971) 1522.
- [2] Y. Le Grand, S.G. El Hage, *Physiological Optics*, Springer, Berlin, 1980.
- [3] A.C. Kooijman, *J. Opt. Soc. Am.* 73 (1983) 1544.
- [4] R. Navarro, J. Santamaria, J. Bescos, *J. Opt. Soc. Am. A* 2 (1985) 1273.
- [5] D.A. Atchison, G. Smith, *Optics of the Human Eye*, Butterworth-Heinemann, Oxford, 2000.
- [6] P.J. Sands, *J. Opt. Soc. Am.* 60 (1970) 1436.
- [7] J.G. Sivak, *Am. J. Optom. Physiol. Opt.* 62 (1985) 299.
- [8] H.L. Liou, N.A. Brennan, *J. Opt. Soc. Am. A* 14 (1997) 1684.
- [9] G. Smith, D.A. Atchison, *Ophthal. Physiol. Opt.* 21 (2001) 317.
- [10] A. Gullstrand, *Helmholtz's Physiological Optics*, Optical Society of America, New York, 1924, Appendix, p. 350.
- [11] O. Pomerantzeff, M. Pankratov, G.J. Wang, P. Dufault, *Am. J. Optom. Physiol. Opt.* 61 (1984) 166.
- [12] T. Raasch, V. Lakshminarayanan, *Ophthal. Physiol. Opt.* 9 (1989) 61.
- [13] I.H. Al-Ahdali, M.A. El-Messierly, *Appl. Opt.* 34 (1995) 5738.
- [14] S. Nakao, T. Ono, R. Nagata, K. Iwata, *Jpn. J. Clin. Ophthal.* 23 (1969) 903.
- [15] J.W. Blaker, *J. Opt. Soc. Am.* 70 (1980) 220.
- [16] B.K. Pierscionek, D.Y.C. Chan, *Optom. Vision Sci.* 66 (1989) 822.
- [17] G. Smith, B.K. Pierscionek, D.A. Atchison, *Ophthal. Physiol. Opt.* 11 (1991) 359.
- [18] G. Smith, D.A. Atchison, B.K. Pierscionek, *J. Opt. Soc. Am. A* 9 (1992) 2111.
- [19] D.A. Atchison, G. Smith, *Vision Res.* 35 (1995) 2529.
- [20] G. Smith, D.A. Atchison, *J. Opt. Soc. Am. A* 14 (1997) 2537.
- [21] S. Nakao, S. Fujimoto, R. Nagata, K. Iwata, *J. Opt. Soc. Am.* 58 (1968) 1125.
- [22] W.S. Jagger, *Vision Res.* 30 (1990) 723.
- [23] A. Popiolek-Masajada, H.T. Kasprzak, *Optom. Vision Res.* 76 (1999) 720.
- [24] H.T. Kasprzak, *Ophthal. Physiol. Opt.* 20 (2000) 31.
- [25] G. Smith, *Clin. Exp. Optom.* 86 (2003) 3.
- [26] M.V. Pérez, C. Bao, M.T. Flores-Arias, M.A. Rama, C. Gómez-Reino, *J. Opt. A* 5 (2003) S293.
- [27] R.K. Luneburg, *Mathematical Theory of Optics*, University of California Press, Berkeley, 1964.
- [28] J.F. Koretz, C.A. Cook, *Optom. Vision Sci.* 78 (2001) 396.
- [29] B.A. Moffat, D.A. Atchison, J.M. Pope, *Optom. Vision Sci.* 79 (2002) 148.
- [30] M.S. Sodha, A.K. Gathak, *Inhomogeneous Optical Waveguides*, Plenum Press, New York, 1977.
- [31] W.M. Rosenblum, J.W. Blaker, M.G. Block, *Am. J. Optom. Physiol. Opt.* 65 (1988) 661.
- [32] C. Gómez-Reino, *Int. J. Optoelectron.* 7 (1992) 607.
- [33] W.N. Charman, *Ophthal. Optician* 21 (1981) 72.
- [34] E. Yebra-Pimentel, M.J. Giraldez, J.M. Gonzalez-Mejome, A. Cerviño, C. Garcia-Resua, M.A. Parafita, *Arch. Soc. Esp. Oftalmol.* 79 (2004) 317.